

## Major and trace element composition of the depleted MORB mantle (DMM)

Rhea K. Workman<sup>a,\*</sup>, Stanley R. Hart<sup>b,1</sup>

<sup>a</sup>MIT-WHOI Joint Program, Marine Geology and Geophysics, Woods Hole Oceanographic Institution, Woods Hole, MA 02543, USA

<sup>b</sup>Department of Geology and Geophysics, Woods Hole Oceanographic Institution, Woods Hole, MA 02543, USA

Received 4 May 2004; received in revised form 1 December 2004; accepted 8 December 2004

Available online 20 January 2005

Editor: R.D. van der Hilst

### Abstract

We derive an estimate for the chemical composition of the depleted MORB mantle (DMM), the source reservoir to mid-ocean ridge basalts (MORBs), which represents at least 30% the mass of the whole silicate Earth. A database for the chemical and physical properties of abyssal peridotites has become robust and complete enough to truly access a reference DMM. Using trace element depletion trends from the abyssal peridotites, it is possible to construct a large part of DMM's trace element pattern. Splicing this information with isotopic constraints (Sr–Nd–Pb–Hf) and canonical ratios (Ce/Pb, Nb/Ta, Nb/U, Ba/Rb, H<sub>2</sub>O/Ce, CO<sub>2</sub>/Nb and Cl/K), we can extend abundance estimates to all the incompatible elements including volatile content. The resulting trace element pattern for average DMM constrains parental MORB to be generated by 6% aggregated fractional melting, consistent with recent models for hydrous melting of the mantle [P.D. Asimow, J.E. Dixon, C.H. Langmuir, A hydrous melting and fractionation model for mid-ocean ridge basalts: application to the Mid-Atlantic Ridge near the Azores, *Geochem. Geophys. Geosyst.* 5 (2004) 10.1029/2003GC000568]. We show that DMM is roughly balanced by the continental crust and better balanced upon inclusion of ocean island basalt source and oceanic crust components. Compared to the primitive mantle, DMM has been depleted by 2–3% melt extraction and has only 15% the radiogenic heat production.

© 2004 Elsevier B.V. All rights reserved.

*Keywords:* DMM; major elements; trace elements; mid-ocean ridge basalts; mantle

### 1. Introduction

The trace element composition of the depleted upper mantle (DMM) is a fundamental parameter in

modeling the generation of mid-ocean ridge basalts (MORBs), calculating the crust–mantle mass balance, and establishing the chemical and thermal evolution of the Earth. To date, all attempts to establish an average composition for the upper mantle, whether by parent/daughter derivations from isotopic systems [1–6] or by MORB trace element inversions [6–9], have centered on MORB liquids and included major

\* Corresponding author. Tel.: +1 508 289 2467.

E-mail addresses: [rworkman@whoi.edu](mailto:rworkman@whoi.edu) (R.K. Workman), [shart@whoi.edu](mailto:shart@whoi.edu) (S.R. Hart).

<sup>1</sup> Tel.: +1 508 289 2837.

assumptions about melt generation, melt transport, and differentiation processes that have affected these upper mantle melts. Unfortunately, it is just these processes that we are trying to understand, rather than assume a priori.

The most compelling evidence for upper mantle depletion comes from the heavy-element isotopic composition of MORBs. Although MORBs and their residues, abyssal peridotites, have some degree of heterogeneity in radiogenic isotope ratios (Sr–Nd–Pb–Hf), they are focused within a small range of values relative to ocean island basalts and are, with very few exceptions, depleted from bulk earth values in  $^{87}\text{Sr}/^{86}\text{Sr}$ ,  $^{143}\text{Nd}/^{144}\text{Nd}$ , and  $^{176}\text{Hf}/^{177}\text{Hf}$ , thus requiring a long-term history of low Rb/Sr, Hf/Lu, and Nd/Sm (i.e. incompatible element depletion). Direct evidence for upper mantle depletion came with the classic trace element studies of Johnson et al. [10] and Johnson and Dick [11] on abyssal peridotites, but most of the observed depletion in these peridotites is due to melt extraction during the latest spreading events, so that the composition of the general ambient upper mantle has been severely overprinted by this latest melting episode.

Ultimately, we know that this mantle, which has been estimated to comprise 30–70% by mass of the bulk silicate earth, has been depleted over time in the highly incompatible (lithophile) elements ([1,8], refs. therein). Most models ascribe the depletion of the upper mantle to the extraction of the enriched continental crust, a process that has removed up to 90% of the most incompatible elements, and 80–85% of the heat-producing elements (e.g. [8]). Some part of the depletion may also be created by the preservation of recycled oceanic crust that is currently sequestered in unknown regions of the mantle. It is possible the lower mantle (below 670 km) has also been depleted by such processes, but this question is highly controversial at present.

In place of assuming a set of bulk partition coefficients or a degree of melt extraction, we use in this paper the following constraints in deriving an average trace element composition of DMM: (1) trace element content of clinopyroxenes from abyssal peridotites, (2) isotopic evolution from primitive upper mantle (PUM), and (3) canonical trace element ratios in MORBs. Abyssal peridotite data from the literature, the backbone of this study, are treated in a way reminiscent of studies such as Loubet et al. [12], Hart and Zindler [13], and McDonough and Sun [14]. Abyssal perido-

tites, unlike basalts, are not modified by secondary processes such as fractional crystallization, magma mixing, and crustal assimilation [15], but may be subject to melt impregnation [16] and melt/rock reaction [17]. We show that melt impregnation can be recognized and therefore filtered from the abyssal peridotite data set and suggest that melt/rock reaction in the data set we have used has had more effect on major element chemistry than trace element chemistry. Overall, it seems that, for the moderately incompatible elements, abyssal peridotites more accurately record the trend of upper mantle depletion than do MORBs.

The average trace element content of DMM, as deduced here, generally shows a very smooth pattern with increasing trace element compatibility, which to first order mass-balances with the continental crust. The degree of depletion indicated in DMM represents 2–3% melt removal from the primitive upper mantle (PUM) of McDonough and Sun [14]; this means that DMM has only 15% the radiogenic heat production of PUM (from K, U, and Th). Present-day ocean crust (i.e. MORBs) can be modeled with 6% aggregated fractional melting of the deduced DMM.

## 2. Trace element composition of DMM

### 2.1. Abyssal peridotites

Abyssal peridotites have been shown to be residues of fractional or near-fractional melting that produces MORB (e.g. [10]). Although bulk trace element compositions of these peridotites are heavily modified by alteration on the seafloor, many workers have analyzed the trace element compositions (Sr, Zr, Ti, Ce, Nd, Sm, Eu, Gd, Dy, Er, Yb, and Y) of relict, unaltered clinopyroxene grains as a means of chemical characterization [10,11,18–21]. Using such clinopyroxene compositions, bulk compositions ( $C_{\text{WholeRock}}$ ) of the peridotites can be calculated for each trace element with the following equation:

$$C_{\text{WholeRock}} = C_{\text{cpx}} \left( \frac{D_{\text{bulk}}}{D_{\text{cpx}}} \right) \quad (1)$$

Where the bulk partition coefficient ( $D_{\text{bulk}}$ ) is determined from modal abundances ( $x_{\text{mineral}}$ ) of olivine (ol), orthopyroxene (opx), clinopyroxene (cpx), and spinel

(sp), and mineral/melt partition coefficients ( $D_{\text{mineral}}$ ) as follows:

$$D_{\text{bulk}} = x_{\text{ol}}D_{\text{ol}} + x_{\text{opx}}D_{\text{opx}} + x_{\text{cpx}}D_{\text{cpx}} + x_{\text{sp}}D_{\text{sp}} \quad (2)$$

This method of calculating bulk peridotite compositions is a substitute for a more accurate method, which would be to sum the concentrations of trace elements in minerals according to their modal proportions. Converting to whole rock compositions from clinopyroxene alone is done simply due to the fact that almost no trace element data exist for other minerals in the peridotite samples.

We have compiled a data set from the literature that includes abyssal peridotites having both cpx trace element analyses and modal abundances (data sources are [10,11,15,18–21]). All samples containing more than 1% modal plagioclase are excluded on the basis that most plagioclase in abyssal peridotites has been interpreted as a secondary phase representative of melt impregnation [16,21]; as a result, only 5 out of almost 90 samples included have any reported modal plagioclase at all. Anomalously high Ce and Sr values have also been excluded for some samples. For Sr, some anomalous values are suspected seawater alteration; such Sr anomalies are not accompanied by Eu

anomalies and therefore are not suspected to be plagioclase reaction products. For both Sr and Ce, the most incompatible elements of the sample suite and therefore the most depleted in abyssal peridotites, elevated concentrations are probably due to small amounts of melt impregnation (see discussion below).

The final trace element data set for the abyssal peridotites, corrected to whole rock compositions using mineral/melt partition coefficients from Kelemen et al. [22], published modal abundances and the above equations, is shown in Fig. 1 and can be obtained in Appendix A. It is important to note that the geographical distribution of the sample suite is highly focused on the Southern Ocean; 90% of the samples originate from the American–Antarctic, Southwest Indian and Central Indian Mid-Ocean Ridges, with the remaining 10% obtained from the Mid-Atlantic Ridge and East Pacific Rise. The question of whether or not this geographical bias manifests as a chemical bias will not be answered until larger data sets from other localities are established.

The purpose of compiling bulk rock information is to derive the inter-relationships between different trace elements (i.e. to what degree the various incompatible

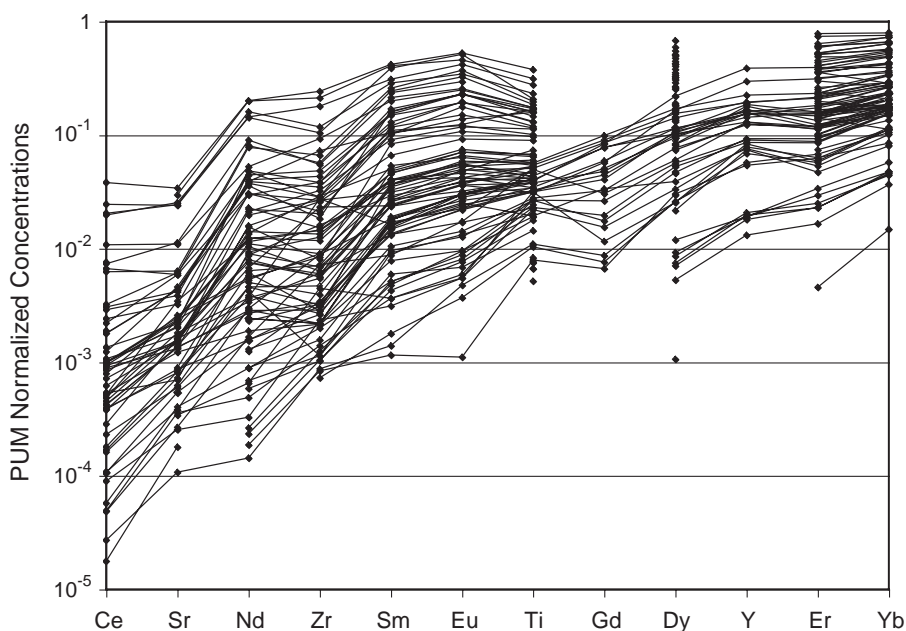


Fig. 1. Calculated whole rock trace element compositions of abyssal peridotites. Data can be found in Appendix A; data sources as quoted in the text.

trace elements are depleted relative to each other over the entire history of mantle depletion). A formulation of the trace element “system” begins by interpreting the trace element compositions of peridotites using the equation for a residue of fractional melting (see Zou [23] for review of melting models). Calculations show that modal fractional melting used to interpret residues of melting is a fine approximation for any number of more complicated melting models (see Appendix A). The ratio of the concentration of a given element in a solid,  $C_s$ , to its original concentration,  $C_o$ , after some fraction of melting,  $F$ , is as follows:

$$\frac{C_s}{C_o} = (1 - F)^{\left(\frac{1}{D} - 1\right)} \quad (3)$$

Where  $D$  is the bulk solid/melt partition coefficient for modal melting.

The relationship between the concentrations of two elements in the residue,  $[A]$  and  $[B]$ , can be linearized upon equating two equations solved for  $F$ :

$$\ln(C_s^A) = R \ln(C_s^B) + \ln\left(\frac{C_o^A}{(C_o^B)^R}\right) \quad (4)$$

Where the slope,  $R$ , on the linear  $\ln([A])$  vs.  $\ln([B])$  array is a function of the bulk partition coefficients for elements  $A$  and  $B$ :

$$R = \frac{D_B(1 - D_A)}{D_A(1 - D_B)} \quad (5)$$

Given that we have information for 12 different elements (see Fig. 1), there are 132 of the  $\ln([A])$  vs.  $\ln([B])$  relationships to consider in the overall reduction of this data set; Fig. 2 shows a sampling of these linear arrays, with the more incompatible of a given element pair plotted on the  $x$ -axis. The peridotites show an extremely wide range in degree of depletion and form well-correlated depletion trends for upper mantle melting. Correlations are best for those element pairs having similar bulk  $D$  values (see the Sm–Nd, Sm–Eu and Dy–Er panels in Fig. 2), and fall off slightly for elements with increasingly dissimilar bulk  $D$ 's (see Zr–Ti and Sm–Yb). Some of the scatter in correlations may have been produced by melt impregnation. For instance, impregnation of low degree melts into highly depleted residues would cause points to fall off the

depletion trends toward the more incompatible element, as shown in Fig. 2. Melt impregnation trajectories for relationships among the HREE (e.g. Dy–Er) very closely overlap their well-correlated arrays (not shown for clarity), thereby indicating that melt impregnation has none to very little effect on the slopes or positions of these depletion trends.

The  $\ln([A])$  vs.  $\ln([B])$  depletion trends have been fit by a York [24] two-error regression (Fig. 2), assuming a blanket error of 10% for all points. The regressions have also been forced through the primitive upper mantle (PUM) coordinate of McDonough and Sun [14]; most regressions intersect the PUM coordinate without forcing, but this treatment becomes appropriate for some regressions with poor correlations (for example, see the Ce–Nd panel in Fig. 2) and we find it necessary for obtaining robust output from the regression scheme.

The upper mantle is certainly not a unique composition (isotopic or otherwise), but rather a range of compositions reflecting variable amounts of depletion and/or re-enrichment. A given peridotite's bulk trace element composition represents the culmination of melt depletion and enrichment over the entire history of that peridotite. Also, integrated within the trace element trends (Fig. 2) is the net transfer of material out of the mantle by oceanic and continental crust generation as well as crustal recycling, in so far as the recycled material is well mixed within the upper mantle. In this sense, some of the more complicated processes affecting upper mantle composition are incorporated into the abyssal peridotite trends, but are not required to explain the trace element data.

Knowing that much of the depletion observed in abyssal peridotites is caused by the most recent melting event, we need to define where today's average, unmelted upper mantle lies on the depletion trends. For this we need another constraint, the most obvious being the isotopic evolution of DMM: calculating the present-day Sm/Nd ratio from  $^{143}\text{Nd}/^{144}\text{Nd}$  signatures in MORBs defines a unique position on the abyssal peridotite depletion trends.

## 2.2. Isotope constraints

Although there has been much written on the homogeneity of MORBs relative to OIBs [25–27], it is clear from the global database (Fig. 3) that the

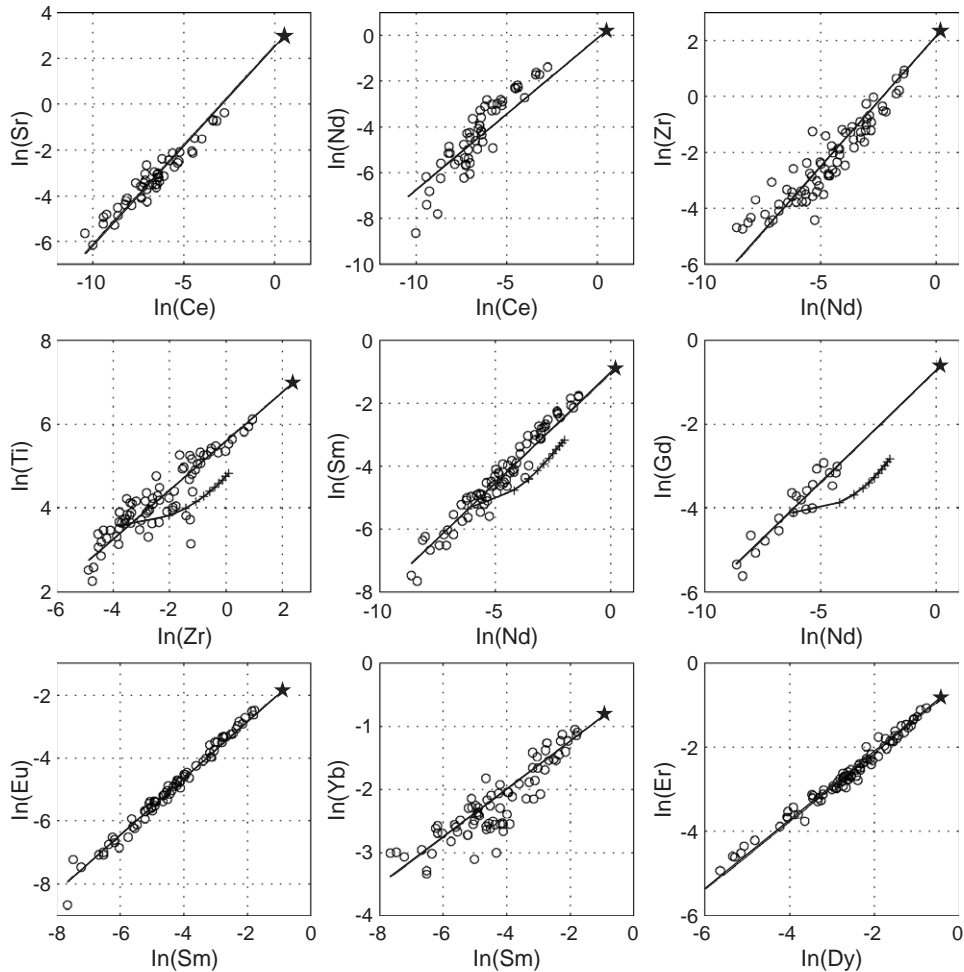


Fig. 2. Co-variation diagrams for trace elements in abyssal peridotites, plotted as  $\ln[A]$  against  $\ln[B]$  in accordance with Eq. (4); the more incompatible element is on the  $x$ -axis for each plot. Star symbol is Primitive Upper Mantle (PUM; also Bulk Silicate Earth, BSE) of McDonough and Sun [14]. Solid line is the best-fit regression, forced through the PUM coordinate and with assigned errors of 10% for each point. The curved lines with crosses (in the middle three panels) are trajectories for impregnation of a 1% melt of DMM (see Fig. 7;  $D$  values from Kelemen et al. [22]) into a depleted mantle of composition indicated by the points of origin on the regression lines; ticks are in increments of 0.1% up to a total of 1% melt impregnation.

MORB mantle is not one sole isotopic composition and by inference not one sole trace element composition. The variation in MORB  $^{87}\text{Sr}/^{86}\text{Sr}$ ,  $^{143}\text{Nd}/^{144}\text{Nd}$ , and  $^{206}\text{Pb}/^{204}\text{Pb}$  compared to all oceanic basalts is 18%, 35%, and 47%, respectively. To address this issue of compositional heterogeneity in the upper mantle we derive three different trace element compositions for the MORB source by calculating present-day parent/daughter ratios from isotopic signatures and relating those ratios to the abyssal

peridotite depletion trends. A study by Su and Langmuir [28], who have filtered global MORB data for proximity to subduction zones and known plumes/hot spots (Fig. 3; Table 1), provides an average MORB isotopic composition (Sr–Nd–Pb) as well as a standard deviation of the isotope data. We use the Su and Langmuir [28] data analysis to define the following: (1) the average DMM composition, (2) an E-DMM based on isotopes that are  $2\sigma$  enriched over the average, and (3) a D-DMM based on isotopes

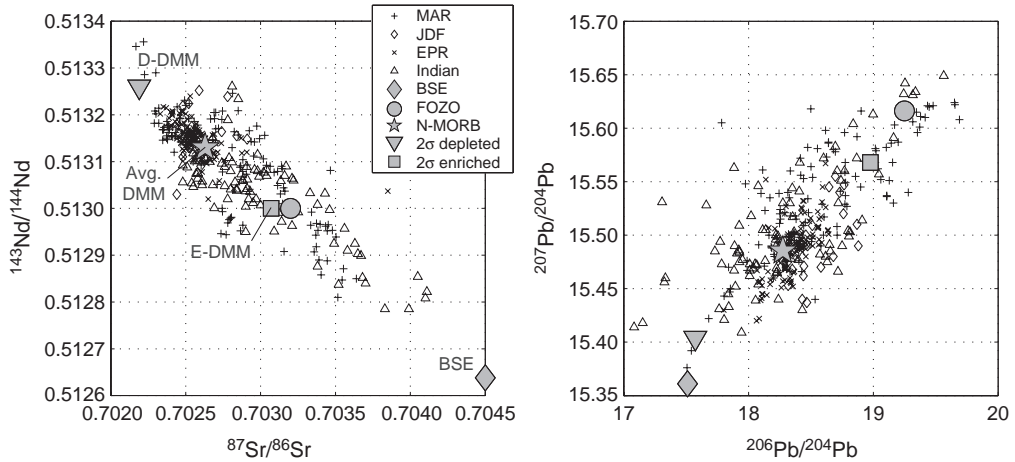


Fig. 3. Two panels showing the Sr–Nd–Pb isotopic compositions of global MORB data obtained from the PETDB database (<http://petdb.ldeo.columbia.edu/petdb/>). MAR–Mid-Atlantic Ridge; JDF–Juan de Fuca Ridge; EPR–East Pacific Rise; Indian–Indian Ocean ridge systems; BSE–Bulk Silicate Earth; FOZO–Focus Zone [74]; N-MORB is the average composition for normal MORBs according to Su and Langmuir [28]. The variation in N-MORB  $^{87}\text{Sr}/^{86}\text{Sr}$ ,  $^{143}\text{Nd}/^{144}\text{Nd}$ , and  $^{206}\text{Pb}/^{204}\text{Pb}$  compared to all of oceanic basalts is 18%, 35%, and 47%, respectively.

that are  $2\sigma$  depleted from the average. The  $^{176}\text{Hf}/^{177}\text{Hf}$  value of DMM is selected by averaging MORB values from Nowell et al. [29], Chauvel and Blichert-Toft [30], and Andres et al. [31];  $^{176}\text{Hf}/^{177}\text{Hf}$  values for E-DMM and D-DMM are based on correlations with  $^{143}\text{Nd}/^{144}\text{Nd}$  (e.g. [30]).

Table 1  
Isotopic constraints on the depleted MORB mantle (DMM)

	BSE <sup>a</sup>	DMM <sup>b</sup>	D-DMM	E-DMM	$\lambda$
$^{87}\text{Sr}/^{86}\text{Sr}$	0.7045	0.70263	0.70219	0.70307	$1.42 \times 10^{-11}$
$^{143}\text{Nd}/^{144}\text{Nd}$	0.512638	0.51313	0.51326	0.51300	$6.54 \times 10^{-12}$
$^{176}\text{Hf}/^{177}\text{Hf}$	0.28276	0.28326	0.28350	0.28310	$1.876 \times 10^{-11}$
$^{206}\text{Pb}/^{204}\text{Pb}$	17.511	18.275	17.573	18.977	$1.55125 \times 10^{-10}$
$^{207}\text{Pb}/^{204}\text{Pb}$	15.361	15.486	15.404	15.568	$9.8485 \times 10^{-10}$
Rb/Sr <sup>c</sup>	0.0307	0.0065	0.0033	0.0111	
Sm/Nd	0.325	0.411	0.435	0.388	
Lu/Hf	0.239	0.369	0.439	0.325	
U/Pb	0.130	0.172	0.131	0.217	
Th/U <sup>d</sup>	3.9	2.5	2.2	3.0	

<sup>a</sup> Age of Earth=4.55 Ga.

<sup>b</sup> Sr–Nd–Pb isotopic compositions taken from Su and Langmuir [28]; DMM is their average for MORBs far from plumes, D-DMM is  $2\sigma$  depleted and E-DMM is  $2\sigma$  enriched over the average. See text for Hf isotope references.

<sup>c</sup> Present-day parent/daughter ratios, calculated with a continuous depletion model starting 3 Ga. Decay constants ( $\lambda$ 's) are summarized in Dickin [77].

<sup>d</sup> Th/U ratios taken from U-Series disequilibrium studies on MORBs, as quoted in text.

To derive present-day parent/daughter ratios, a depletion model must be assumed. It is common to use a two-stage evolution model with a single, instantaneous depletion event at a time ( $t$ ) equal to the average age of the continental crust. An example from the Rb–Sr system, where  $T$  is the age of the Earth and parent/daughter ratios are for present-day is the following:

$$\begin{aligned} \left(\frac{^{87}\text{Sr}}{^{86}\text{Sr}}\right)_{\text{DMM}} &= \left(\frac{^{87}\text{Sr}}{^{86}\text{Sr}}\right)_0 \\ &+ \left(\frac{^{87}\text{Rb}}{^{86}\text{Sr}}\right)_{\text{BSE}} (e^{\lambda T} - e^{\lambda t}) \\ &+ \left(\frac{^{87}\text{Rb}}{^{86}\text{Sr}}\right)_{\text{DMM}} (e^{\lambda t} - 1) \end{aligned} \quad (6)$$

However, because mantle depletion is largely the result of continental crust extraction, it is important to consider continental growth through time and the fact that it is not a single depletion event as modeled in the above equation. Although there is debate about continuous growth [32] or constant volume with crustal recycling [33–35], somewhere in between (such as episodic growth) is probably the reality [36–38]. Models suggesting continuous growth generally agree that the real increase in continental mass was at about 3 Ga [37]. Models in favor of constant crustal volume suggest rapid (or at least effective) recycling of crust

greater than 3 billion years old (e.g. [34,39]). For our purpose, it is really preservation that is of issue; even though there are isotopic arguments for a 4.0 Ga depleted mantle of similar size and degree of depletion as the modern depleted mantle (e.g. [39,40]), it is more important here that the abundance of that old crust is low compared to crust younger than 3.0 Ga. Isotopically, the recycling of old crust would make depletion appear to be younger on average and smear out (or even negate) the signal of ancient depletion.

Here we have improved on the classical methods by using a continuous transport, melt depletion model starting at 3 Ga. The equation for the Sr isotopic composition of DMM at time,  $t$ , as derived by Allègre [41] and Hart and Brooks [42] is:

$$\left(\frac{^{87}\text{Sr}}{^{86}\text{Sr}}\right)_t = \left(\frac{^{87}\text{Sr}}{^{86}\text{Sr}}\right)_o + \frac{\lambda(^{87}\text{Rb}/^{86}\text{Sr})_o [1 - e^{-(\lambda+k)t}]}{\lambda + k} \quad (7)$$

where  $\lambda$  is the decay constant for  $^{87}\text{Rb}$  and  $k$  is the difference in transport coefficients between Rb and Sr

and essentially relates to the difference between bulk partitioning of the two elements. The initial conditions are values for bulk silicate Earth at the time when depletion begins (3.0 Ga). The parameter,  $k$ , is solved for by knowing the isotopic composition of bulk Earth at 3 Ga and DMM at time zero (i.e. present-day), as shown in Table 1. The parent/daughter variation through time is then:

$$\left(^{87}\text{Rb}/^{86}\text{Sr}\right)_t = \left(^{87}\text{Rb}/^{86}\text{Sr}\right)_o e^{-(\lambda+k)t} \quad (8)$$

Fig. 4 shows how this model, as used for the Rb/Sr system, gives a factor of  $\sim 2$  lower estimate for the present-day Rb/Sr ratio of DMM, compared to the usual two-stage model. Decreasing the age of depletion requires lower Rb/Sr ratios for the same present-day  $^{87}\text{Sr}/^{86}\text{Sr}$  ratio. In the same way that the Sr isotopes are used to constrain the Rb/Sr ratio of DMM, similar constraints result in determinations for Sm/Nd, Lu/Hf, and U/Pb (Table 1). The choice of depletion model does not greatly affect the Sm–Nd system, but is important for the whole suite of parent/daughter ratios.

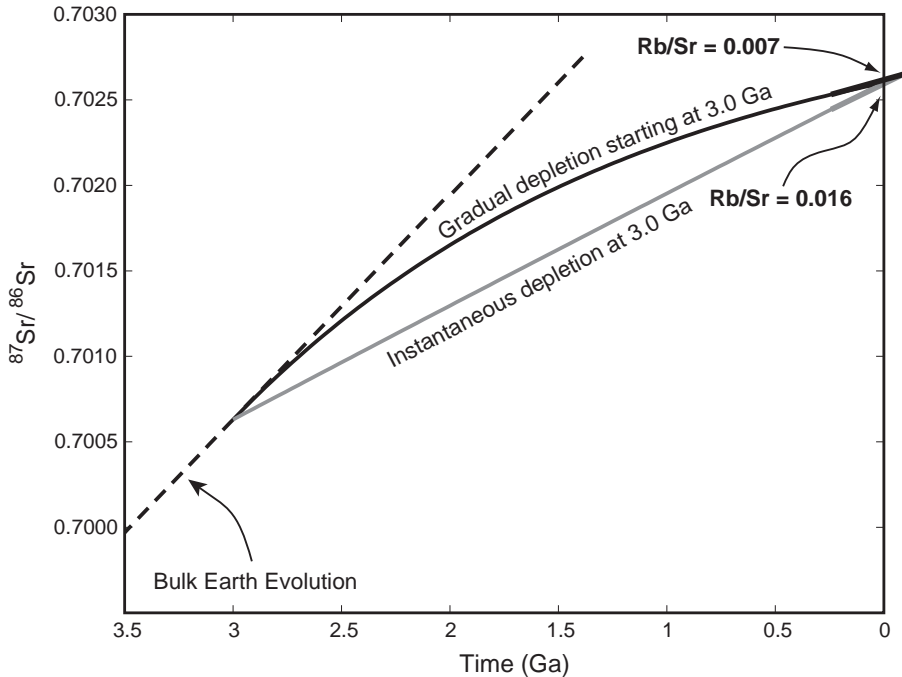


Fig. 4. Plot showing examples of instantaneous depletion and continuous depletion models for the isotopic evolution of Sr in DMM. Note that the derived Rb/Sr ratio of today's upper mantle varies by a factor of about two between the models—the Rb/Sr ratio is defined by the slope of the evolution curves. Nd isotopic evolution by continuous depletion is not shown since it is essentially linear through time. See Table 1 for isotope evolution parameters and Eqs. (7) and (8) for continuous depletion model.

Most important to the abyssal peridotite inversion is the present-day Sm/Nd ratio for DMM, since this identifies the present-day position of DMM on the mantle depletion arrays. Fig. 5 shows how the Sm/Nd ratio of 0.411 in average DMM has a unique intersection with the Sm–Nd abyssal peridotite regression line, defining unique Sm and Nd concentrations of 0.239 ppm and 0.581 ppm, respectively. Given the absolute concentrations of Sm and Nd, we can derive the absolute concentrations of all the other trace elements that have been analyzed in abyssal peridotites (REE, Sr, Zr, Ti, Y; Table 2). Ultimately, estimates for every element concentration are obtained based on relationships with every other element. Standard deviations of various estimates for a given element are on the order of 1–2% for REE's and Ti and 5–6% for Sr, Zr, and Ce, indicating that the depletion trends are internally very consistent; note that these standard deviations do not testify to the accuracy of the model. With other parent/daughter ratios, other pieces of the trace element pattern for DMM are estimated: Rb

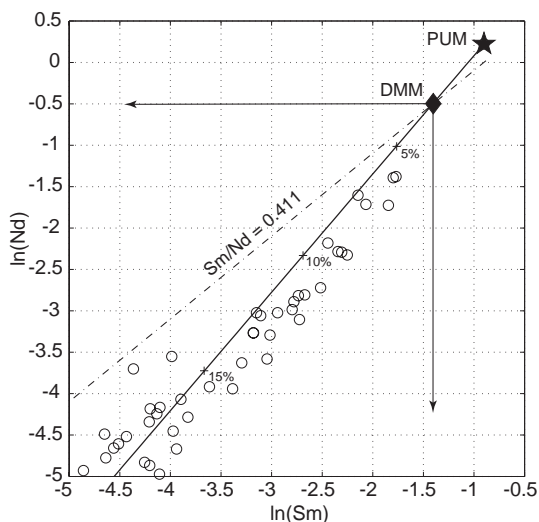


Fig. 5. Plot of  $\ln([Sm])$  vs.  $\ln([Nd])$  of abyssal peridotites showing the upper half of the mantle depletion array (see Fig. 2 for full scale). Star symbol marks the PUM coordinate (i.e. BSE) of McDonough and Sun [14]. Crosses on the mantle depletion line mark percent melt extraction for fractional melting using bulk  $D$  values as reported in Table 2. Line of constant Sm/Nd of 0.411 is derived from the Nd isotopic evolution of DMM; the intersection of this line with the mantle depletion line marks today's average composition of DMM. From Sm and Nd concentrations, concentrations of all other elements reported for abyssal peridotites (see Fig. 1) can be derived from the system of mantle depletion arrays like those shown in Fig. 2.

derives directly from the Sr; Hf derives from extrapolation to Lu from the REE's; Pb derives from the Ce/Pb canonical ratio (see below); and U follows (Table 2). The same procedure is applied with the E-DMM and D-DMM isotopic compositions.

It is possible to derive Th concentrations from Th/U ratios inferred from  $^{208}\text{Pb}/^{204}\text{Pb}$  and  $^{206}\text{Pb}/^{204}\text{Pb}$  isotopic evolution. However, it has been widely recognized that inferred Th/U ratios are generally much higher than observed Th/U ratios in MORBs; this has been termed the 'kappa conundrum' [2,5,43]. Since Th and U are both highly incompatible during mantle melting, with Th being slightly more incompatible, the Th/U ratios of MORBs should provide an upper limit to the source Th/U. Due to the extremely long half-life of  $^{232}\text{Th}$  (14 Byr), we interpret the kappa conundrum to be a problem where the Th–Pb system has not “caught-up” with the U–Pb system. For a more accurate representation of present-day upper mantle, we use Th/U ratios measured by careful U-Series studies on MORBs [44–46] over the range in isotopic composition used to define our D-DMM through to E-DMM (Table 1).

### 2.3. Canonical ratios and volatile contents

There are few trace element ratios in MORBs (as well as many OIBs) that remain constant over variable degree of melting and variable isotopic composition. These ratios (Ce/Pb, Nb/Ta, Nb/U, and Ba/Rb) are termed “canonical” and their constancy is interpreted to be due to bulk partition coefficients being very nearly the same for the element pairs during upper mantle melting, preventing significant fractionation [47–52]. Hence, ratios in the melts are presumed to be identical to ratios of these elements in the source.

We employ these canonical ratios in order to complete the trace element pattern of DMM. It is clear though, from Fig. 6, that some canonical ratios are better behaved than others; Nb/Ta, Nb/U, and Ba/Rb all hover about their published values of 15.5, 47, and 11.3, respectively [47–49,51,52], whereas Ce/Pb ratios display much more scatter with a significant distribution of data higher than either published canonical values of 25 and 20 [48,50]. As a mid-value of the MORB data, we use a Ce/Pb ratio of 30; if, in studies to come, it is determined that Ce/Pb should be lower, we recommend changing only the Pb concentration in

Table 2  
Trace element composition of DMM

	Average DMM (ppm)	Normalized <sup>a</sup>	Range <sup>b</sup>		Enriched DMM (ppm)	Depleted DMM (ppm)	Constraint	Bulk $D^c$	1 $\sigma$ (%)
			Min	Max					
Rb	0.050	0.083	0.023	0.079	0.108	0.020	Isotopes	<i>0.0001</i>	
Ba	0.563	0.085	0.256	0.896	1.219	0.227	Canonical Ratio	<i>0.00012</i>	
Th	0.0079	0.099	0.0068	0.0089	0.0157	0.0040	U-Series	<i>0.001</i>	
U	0.0032	0.156	0.0027	0.0036	0.0052	0.0018	Isotopes	<i>0.0011</i>	
Nb	0.1485	0.226	0.1277	0.1671	0.2462	0.0864	Canonical Ratio	<i>0.0034</i>	
Ta	0.0096	0.259	0.0082	0.0108	0.0159	0.0056	Canonical Ratio	<i>0.0034</i>	
La	0.192	0.296	0.157	0.222	0.253	0.134	Extrapolated	<i>0.01</i>	
Ce	0.550	0.329	0.451	0.639	0.726	0.421	Regression	0.022	3.9
Pb	0.018	0.122	0.015	0.021	0.024	0.014	Canonical Ratio	<i>0.014</i>	
Pr	0.107	0.420	0.091	0.120	0.132	0.087	Interpolated	<u>0.027</u>	
Nd	0.581	0.465	0.507	0.644	0.703	0.483	Regression	0.031	3.6
Sr	7.664	0.385	6.462	8.709	9.718	6.092	Regression	0.025	4.7
Zr	5.082	0.484	4.465	5.601	6.087	4.269	Regression	0.033	7.2
Hf	0.157	0.555	0.142	0.170	0.186	0.127	Isotopes	<u>0.035</u>	
Sm	0.239	0.588	0.217	0.256	0.273	0.210	Regression	0.045	2.2
Eu	0.096	0.624	0.088	0.102	0.108	0.086	Regression	0.050	2.5
Ti	716.3	0.594	666.5	756.1	792.0	650.0	Regression	0.058	2.9
Gd	0.358	0.658	0.332	0.379	0.397	0.324	Regression	0.056	4.5
Tb	0.070	0.704	0.065	0.073	0.076	0.064	Interpolated	<u>0.068</u>	
Dy	0.505	0.749	0.480	0.525	0.543	0.471	Regression	0.079	7.3
Ho	0.115	0.772	0.110	0.119	0.123	0.108	Interpolated	<u>0.084</u>	
Y	3.328	0.774	3.179	3.445	3.548	3.129	Regression	0.088	5.0
Er	0.348	0.795	0.334	0.359	0.369	0.329	Regression	0.097	8.7
Yb	0.365	0.827	0.353	0.374	0.382	0.348	Regression	0.115	8.1
Lu	0.058	0.859	0.056	0.059	0.060	0.056	Extrapolated	<u>0.120</u>	

<sup>a</sup> Normalized to primitive upper mantle (PUM) with values from McDonough and Sun [14].

<sup>b</sup> Minimum and maximum estimates for average DMM concentrations, based on assuming initiation of continuous depletion at 2.5 Ga and 3.5 Ga, respectively.

<sup>c</sup> Bulk partition coefficients calculated from Eq. (5), assuming  $D_{Nd}=0.031$  and solving for all other  $D$ 's; 1 $\sigma$  errors (%) are based on the variation of  $D$  estimates obtained from various regressions involving a given element. Values in italics are from Kelemen et al. [22], except Rb, which is assumed, and U and Th, which are based on our own literature compilation. Underlined values are interpolated between regression outputs.

DMM, as the U–Nb–Ta–La–Ce segment of the trace element patterns derived is consistent with MORB trace element characteristics (see Section 3.2). This would imply that the derived U/Pb ratios from Pb isotopic inversions are not accurate—i.e. that U and Pb cycling in the upper mantle is more complicated than is assumed to be here. All other canonical ratios used are as previously published.

There is also a suite of canonical ratios involving the volatile elements H, C, and Cl that are useful for estimating the budget of these elements in the upper mantle. Volatile elements play an important role in melt generation and transport, so the following estimates are crucial input parameters for modeling such processes. The compatibility of water has been

shown to be similar to that of Ce, and MORBs have on average an H<sub>2</sub>O/Ce ratio of ~200 [53]. Using Ce=0.550 ppm (Table 2), H<sub>2</sub>O is calculated to be 110 ppm in DMM. Using a lower limit of 150 and upper limit of 250 for H<sub>2</sub>O/Ce [53] along with our lower and upper estimates for Ce (Table 2), respectively, the range of water content in DMM is 70–160 ppm.

In a recent study on volatile undersaturated basaltic melt inclusions from the Siqueiros transform fault, Saal [54] have established two new working canonical ratios: CO<sub>2</sub>/Nb at 239±46 and Cl/K at 0.0075±0.0025. Using our Nb min/max estimates from Table 2 and our K estimate from Table 3 (see Section 3.1 below), average DMM has a CO<sub>2</sub> content of 36±12 ppm and a Cl content of 0.38±0.25 ppm. These estimates are about

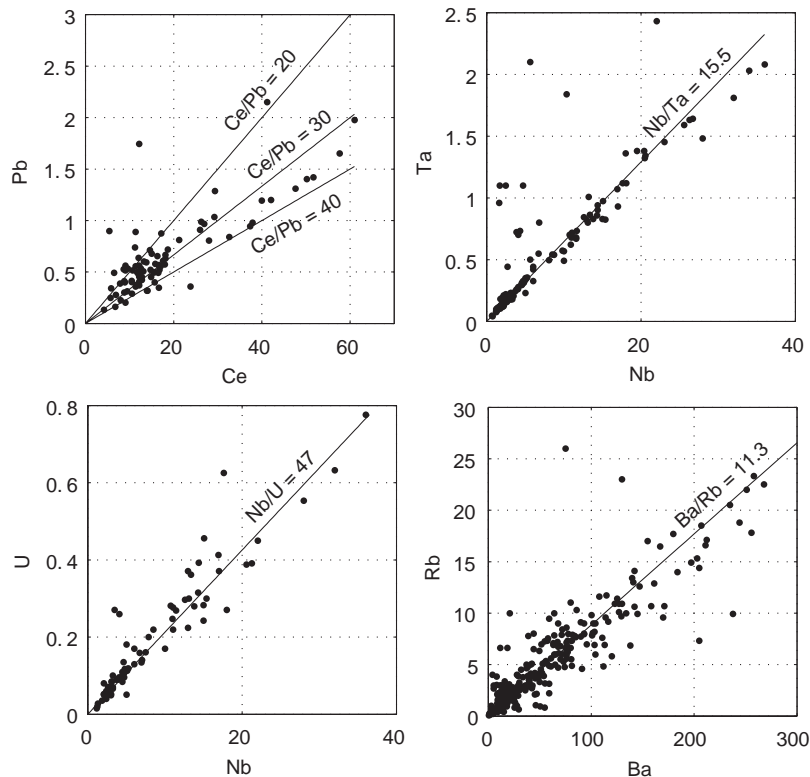


Fig. 6. Four panels showing co-variation plots for elements in MORBs having canonical ratios. Data (in ppm) acquired from the PETDB database (<http://www.petdb.ldeo.columbia.edu/petdb/>). Literature values for canonical ratios (see text for references) are plotted for all panels except Ce–Pb, for which bounding and median values are shown.

2 times lower than those reported by Saal et al. [54] due to their use of different trace element abundances in DMM, but within error of recent estimates by Salters and Stracke [6].

#### 2.4. Final product

Combining the mantle depletion trends from the abyssal peridotites, parent/daughter ratios from the isotopic evolution of DMM, and a handful of canonical ratios, trace element patterns (“spidergrams”) of average DMM, E-DMM (enriched from the average), and D-DMM (depleted from the average) have been derived (Fig. 7a; Table 1 for isotope values; Table 2 for trace element compositions). Overall, the spidergrams are very smooth except for a dip in Sr along with an expected Pb anomaly (see Hofmann, [8]). The greatest difference between the three compositions is in the highly incompatible elements; for example, Rb

and Ba vary by a factor of  $\sim 5$ , but Sm varies by only 30%.

Because it is difficult to assign errors to the estimated compositions, we have provided minimum and maximum estimates for trace element concentrations in the average DMM by using starting ages for the continuous depletion model at 2.5 and 3.5 Ga, respectively (see the grey lines on Fig. 7b; Table 2). By changing the initial assumption of depletion age, we are effectively saying DMM is more or less depleted and all elements together move up or down the depletion arrays in proportion to their compatibilities during melting. Each of these patterns is internally consistent, and therefore not a true range for each element but rather a coherent solution for the assumptions made. It is not advisable to “mix and match” values from different patterns, since the elements behave as a system, not independently, and should be regarded as such. However, the Ba/Th ratios

Table 3  
Modal abundances and major element composition of DMM

	Modal Abundances in DMM (%):				Bulk DMM	PUM <sup>a</sup>	Primary N-MORB <sup>b</sup>	PUM minus 3% N-MORB
	Olivine	Opx	Cpx	Spinel				
	57	28	13	2				
	Mineral compositions:				Bulk DMM	PUM <sup>a</sup>	Primary N-MORB <sup>b</sup>	PUM minus 3% N-MORB
	Olivine	Opx	Cpx	Spinel				
SiO <sub>2</sub>	40.70	53.36	50.61		44.71	44.90	49.51	44.87
Al <sub>2</sub> O <sub>3</sub>		6.46	7.87	57.54	3.98	4.44	16.75	4.07
FeO <sup>c</sup>	10.16	6.27	2.94	12.56	8.18	8.03	8.05	8.05
MnO	0.14	0.12	0.09	0.16	0.13	0.13	0.14	0.13
MgO	48.59	30.55	16.19	19.27	38.73	37.71	9.74	38.68
CaO	0.05	2.18	19.52		3.17	3.54	12.50	3.27
Na <sub>2</sub> O		0.05	0.89		0.13 (0.28) <sup>d</sup>	0.36	2.18	0.30
Cr <sub>2</sub> O <sub>3</sub>		0.76	1.20	10.23	0.57	0.38	0.07	0.39
TiO <sub>2</sub>		0.16	0.63		0.13	0.20	0.90	0.18
NiO	0.36	0.09	0.06	0.24	0.24	0.25	–	–
K <sub>2</sub> O					0.006 <sup>e</sup>	0.029	0.065	0.028
P <sub>2</sub> O <sub>5</sub>					0.019 <sup>f</sup>	0.021	0.095	0.019
Total	100.00	100.00	100.00	100.00	100.00	100.00	100.00	100.00
Mg # <sup>g</sup>	89.5	89.7	90.8	73.2	89.4	89.3	70.6	89.5
Cr # <sup>h</sup>				10.7				
CaO/Al <sub>2</sub> O <sub>3</sub>		0.34	2.48		0.80	0.80	0.75	0.80

<sup>a</sup> Primitive Upper Mantle (PUM) from McDonough and Sun [18].

<sup>b</sup> Primary N-MORB from averaged glass compositions in Presnall and Hoover [78].

<sup>c</sup> Total Fe as FeO.

<sup>d</sup> Value in parentheses is Na<sub>2</sub>O estimated from the mass balance with continental crust (see text).

<sup>e</sup> Calculated by inverting parental N-MORB at 0.1 wt.% K<sub>2</sub>O for 6% melting and assuming  $D_K=0.0013$ .

<sup>f</sup> Calculated by extracting 3% primary N-MORB (shown here) from PUM.

<sup>g</sup> Mg # = molar ratio of Mg/(Mg+Fe<sup>2+</sup>); Mg # of N-MORB uses 90% total FeO as Fe<sup>2+</sup>.

<sup>h</sup> Cr # = molar ratio of Cr/(Cr+Al).

for the 2.5 and 3.5 Ga patterns are, respectively, too high and too low to generate realistic MORB compositions (see Section 3.2) and support the idea that 3.0 Ga is an appropriate assumption for initiation of mantle depletion. As an aside, using a classical 1.8 Ga instantaneous depletion model results in a spidergram (not shown) very similar to that of the 3.5 Ga pattern but with Rb and Ba close to values for the 3.0 Ga (preferred) pattern.

The Salters and Stracke [6] spidergram (Fig. 7b) for average DMM, based on depleted MORB elemental ratios and isotopic evolution, is generally less depleted than the average DMM of this study. In particular, they show significantly higher estimates for the whole left side of the spidergram (Rb to Ce), as well as higher Zr, Hf and Y, than predicted even for our maximum estimate; this is most likely due to their use of an instantaneous

(two-stage) depletion model for isotopic evolution instead of the gradual depletion model described in this paper.

Please note that in the following sections, only average DMM is discussed.

### 3. Physical and chemical properties of DMM

#### 3.1. Modal abundances and major elements

Abyssal peridotites from all over the world show depletion trends not only in trace element content, but also in major element content in the form of modal abundances and mineral compositions [15,18,19,55–57]. In general, these observations are supported by experimental and theoretical studies of peridotite melting [58–61]. With increasing degree of melt

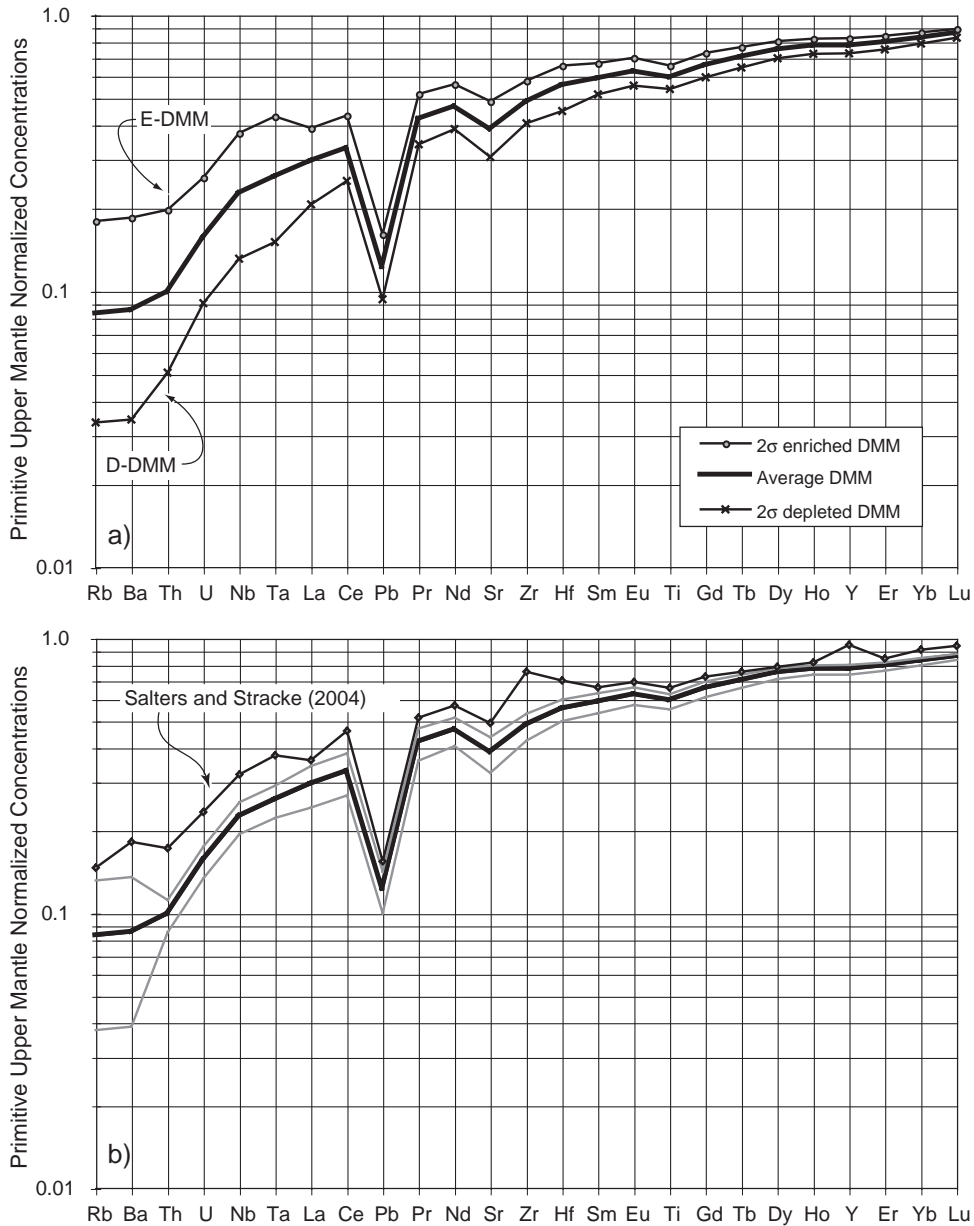


Fig. 7. Panel (a) shows trace element patterns for average Depleted MORB Mantle (DMM), E-DMM, and D-DMM (E- and D- are, respectively, enriched and depleted over the average DMM), as based on a isotopic compositions reported in Table 1). Trace element compositions have been derived from abyssal peridotite depletion trends (see Fig. 2), isotopic evolution based on the average N-MORB Sr–Nd–Pb–Hf isotopic compositions with a gradual depletion model starting at 3 Ga (Table 1; Fig. 3), and canonical ratios (Fig. 6). In panel (b) the upper and lower grey lines result from using gradual depletion models starting at 3.5 Ga and 2.5 Ga, respectively, for the average DMM isotopic composition. The Salters and Stracke [6] trace element pattern for average DMM is shown for comparison.

depletion, olivine increases in modal proportion while orthopyroxene, clinopyroxene, and spinel decrease. Al, Ca, Na, K, and Ti are more incompatible during melting

than Mg, Cr, and Ni, so have the highest mineral and whole rock concentrations in the least depleted peridotites (e.g. [57]).

Since we have established the systematics of incompatible trace elements in abyssal peridotites (see above), we use their relationship to modes to estimate the proportion of minerals in today's average DMM, then challenge the results with considerations of melt extraction and a comparison to the primitive mantle. Using the same data set as employed earlier (obtainable from Appendix A), we have plotted bulk trace element concentrations against modal abundances in individual abyssal peridotites (see examples in Fig. 8); note that these are not completely independent parameters since modes in part determine bulk trace element contents. By extrapolating the trends like those in Fig. 8 to the DMM trace element concentrations (Table 2), we find DMM to be composed of 57% ol, 28% opx, 13% cpx, and 2% sp (Table 3); orthopyroxene does not correlate with any trace elements and has been solved for by summation to 100%. These modes are very close to those found by extrapolating the modal abundance correlations for the South–West Indian Ridge abyssal peridotites [16] for which, without spinel, yields 60% ol, 30% opx, and 10% cpx.

Constructing the bulk depleted mantle composition from mineral modes requires fairly precise knowledge of oxide abundances in the mantle minerals. Baker and Beckett [57] have reduced mineral data for abyssal peridotites and provided algorithms for estimating major element compositions of minerals according to the modal abundance of olivine. Using the Baker and Beckett [57] mineral compositions at 57% olivine and combining the minerals in the given proportions, results in a bulk DMM having an  $\text{Al}_2\text{O}_3$  content nearly that of the primitive upper mantle (PUM; McDonough and Sun [14]), along with a very low Ca/Al ratio compared to PUM. Since Al is depleted during melt extraction and Al is more enriched than Ca in mantle melts (see Table 3), it is reasonable to expect the depleted mantle to have lower Ca and Al concentrations and an equal or higher Ca/Al ratio than that of PUM. This seems to be a problem only with Al abundance and is interpreted to be due to extrapolating mineral compositions beyond the limit of data used by Baker and Beckett [57]. For this reason, we find it more appropriate to use mineral compositions at 60% olivine, the lowermost (i.e. fertile) limit of their regressed data. In doing so, we calculate the major element composition of DMM as reported in Table 3.

Compared to PUM, estimated DMM has, as expected, lower  $\text{SiO}_2$ ,  $\text{TiO}_2$ ,  $\text{Al}_2\text{O}_3$ , CaO,  $\text{Na}_2\text{O}$ , and  $\text{K}_2\text{O}$  with

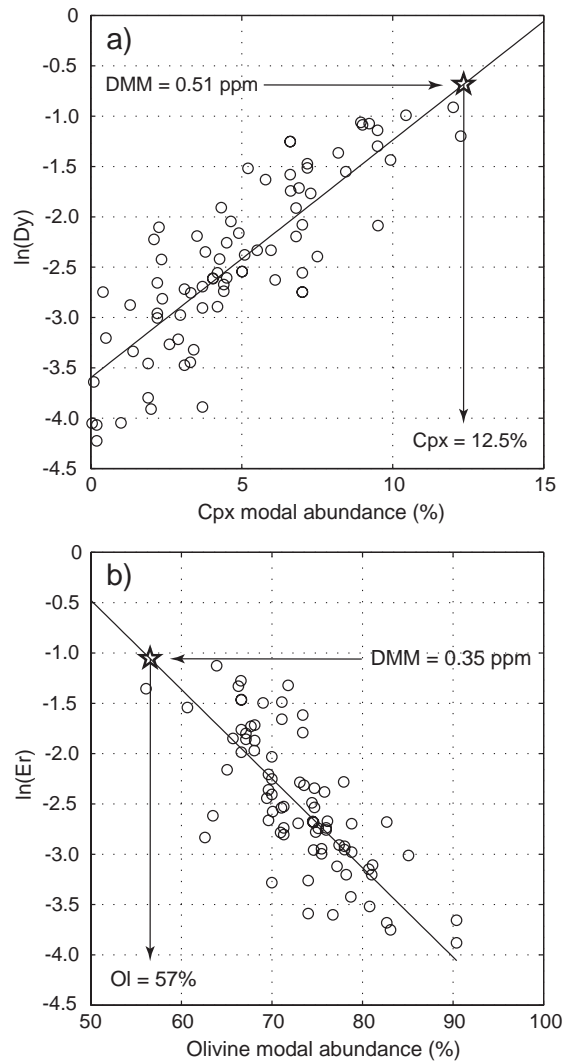


Fig. 8. Modal abundances of (a) clinopyroxene and (b) olivine plotted with calculated (in the same way as for Figs. 1 and 2) bulk trace element compositions of individual peridotites. Determination of the modal composition of DMM results from extrapolating the two-error regressions here to our best estimate for DMM's trace element concentrations (from Table 2).

higher  $\text{MgO}$  and  $\text{Cr}_2\text{O}_3$  (Table 3). The  $\text{TiO}_2$  content of 0.13 wt.% is very close to the 0.12 wt.% calculated from the trace element derivation (Table 2). The  $\text{CaO}/\text{Al}_2\text{O}_3$  ratio is equal to that of PUM (0.80), and would increase to 0.86 by lowering the spinel abundance by only 0.5%. As previously mentioned, much of the trace element depletion in the upper mantle can be attributed to the continental crust. The question now is: can the newly

estimated major element depletion also be attributed to the continental crust? The continental crust budget (see mass-balance section below and bulk continental crust of Rudnick and Fountain [62]) does largely account for the low  $\text{TiO}_2$  and  $\text{K}_2\text{O}$ , the most incompatible of the major elements, and partially accounts for the  $\text{Na}_2\text{O}$ . However, owing to the small mass of continental crust, major elements with less contrast between the crust and mantle cannot be balanced solely by the continents. As a possible solution, Table 3 shows a rudimentary mass balance of the DMM major elements in which 3% of primary MORB is subtracted from PUM (note that this is not a melting model). The major elements calculated in this way show striking similarity to the estimated DMM composition, implying that there is an isolated reservoir of oceanic crust somewhere within the silicate Earth, as also suggested by Hauri and Hart [63]. A second estimate for  $\text{Na}_2\text{O}$  based on mass balance with both the continental crust and a MORB reservoir is also provided in Table 3 and is most likely more accurate than the original sum of mineral compositions.

To convert mineral modes into practical information for those who study abyssal peridotites, we have calculated the trace element composition of the constituent minerals in unmelted, average DMM by using Eqs. (1) and (2) with mineral/melt partition coefficients compiled by Kelemen et al. [22]. This effectively distributes the DMM trace element budget among the minerals according to their relative affinity for incompatible elements. The resulting mineral compositions can be found in Appendix A.

As a cautionary note, the reported modes and mineral compositions will only apply to the very shallow mantle, owing to variable mineral compositions and phases with pressure and temperature, but the average bulk composition of unmelted, upper mantle should be similar at any depth in this reservoir.

### 3.2. MORB generation

Here we present the average DMM trace element composition, so should be able to produce an average parental N-MORB. To model MORB generation, we first calculate bulk partition coefficients ( $D$ ) from Eq. (5) applied to the abyssal peridotite depletion trends. Because the slopes of the depletion trends (Fig. 2) only supply information about ratios of  $D$  values, we initially have to assume a  $D$  for one element and then

calculate the remainder in relation to that one. We have chosen a bulk  $D_{\text{Nd}}$  of 0.031, according to a compilation from Kelemen et al. [22] for upper mantle melting, since the bulk compatibility of Nd is almost identical in both the spinel and garnet facies.

The set of partition coefficients resulting from the inversion of all abyssal peridotite depletion trends is reported in Table 2. Fig. 9 shows the calculated  $D$  values compared to both garnet and spinel facies bulk  $D$ 's from Kelemen et al. [22]; clearly the slope of the calculated  $D$  values very closely matches that of spinel facies melting and is far off the slope of garnet facies melting. Note that choosing a different  $D_{\text{Nd}}$  will change the absolute position but not the slope of the  $D$  values shown in Fig. 9 (meaning the ratios of  $D$ 's will not change). The above observation does not exclude a contribution of trace elements from small degree melts in the garnet facies, especially for elements with low  $D$  values; this may be why Sr and Ce are a little lower than the spinel facies prediction. For elements with higher bulk  $D$ 's in the garnet facies, the majority of depletion will happen in the spinel facies, thus is reflected in the depletion arrays. If depletion for the middle to heavy REE's was significant in garnet melting, the trace element pattern across the REE would be steeper, even if the last  $D$  values to act on the peridotites were those of spinel melting. This is a straightforward effect of fractional melting on residues.

As an average MORB trace element pattern to be fit by our modeling, we use the parental (fractionation-corrected) N-MORB reported by Su and Langmuir [28]. A point generally agreed upon, and hence applied here, is that MORBs are aggregated fractional or near-fractional melts over a range of pressures, as initially confirmed by Sobolev and Shimizu [64]. The highly incompatible elements are enriched ~16-fold over DMM, thus requiring 6% aggregated fractional melting of DMM. Fig. 10 shows the excellent fit to N-MORB using the  $D$  values derived here and reported in Table 2.

The 6% degree of melting to generate MORB is on the low side of previous estimates ranging from 6–20% [65,66]. A higher  $F$  could be obtained if a greater fractionation correction is applied to the already-corrected parental N-MORB of Su and Langmuir [28] since  $F$  is mainly limited by the concentration of highly incompatible elements (i.e. Rb, Ba, U, Th, Nb,

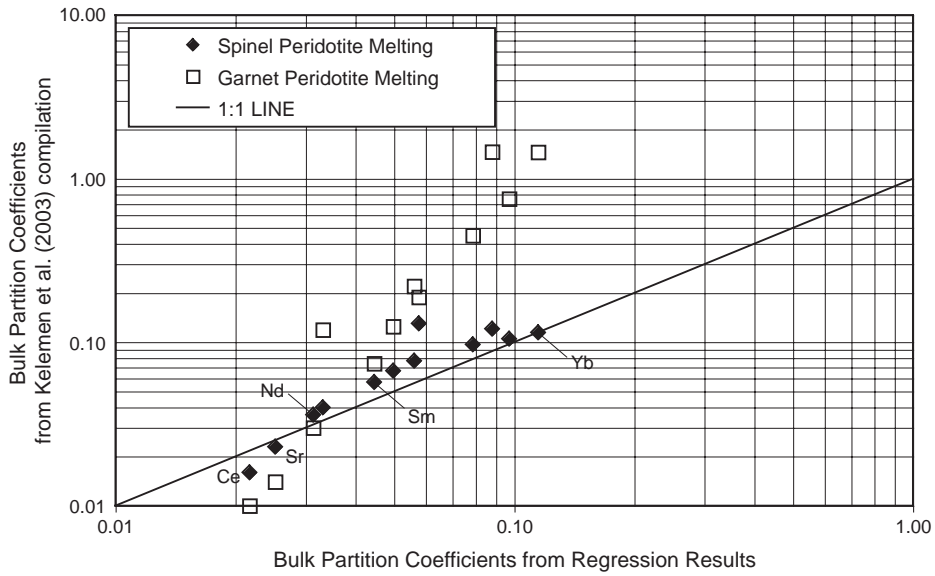


Fig. 9. Bulk partition coefficients ( $D$ 's) as obtained from abyssal peridotite trends (Fig. 2; Table 2) plotted against both spinel and garnet facies bulk  $D$  values from Kelemen et al. [22]. Regression-based  $D$  values are calculated with Eq. (5) and assuming  $D_{Nd}=0.031$ . It is clear that the slope of the  $D$  values obtained reflect melting more in the spinel facies than the garnet facies, as the garnet facies is much steeper. Another choice for  $D_{Nd}$  will change the absolute values, but not the slope, of the points plotted here.

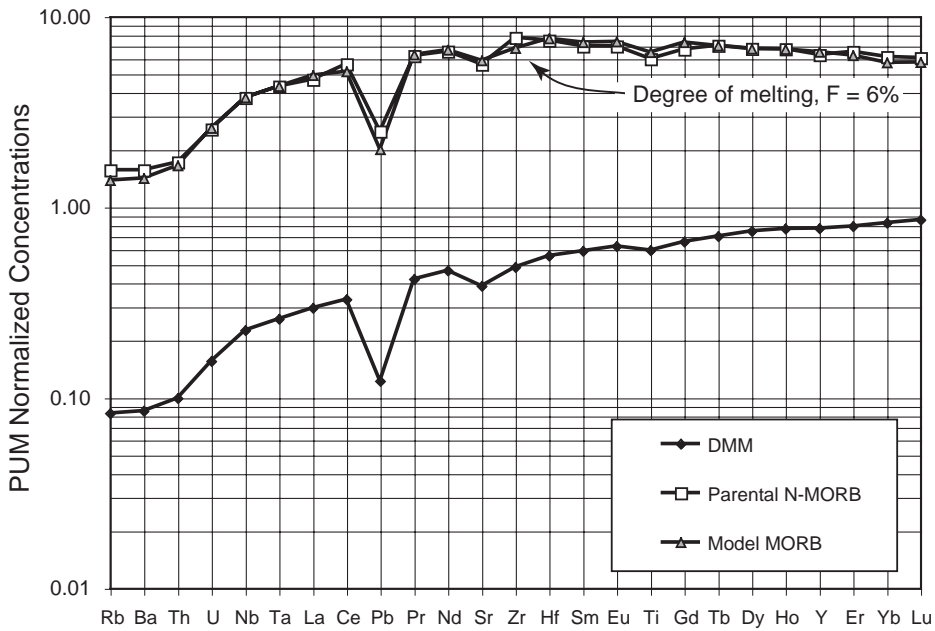


Fig. 10. Plot showing the spectacular fit of parental N-MORB (from Su and Langmuir [28]) by 6% aggregated fractional melting of DMM (from this study) using bulk  $D$  values in Table 2. The Rb, Ba, Th, U, and Pb for the parental MORB are taken from the N-MORB average of Hofmann [8] and adjusted according to fractionation corrections provided by Su and Langmuir [28].

Ta) in the modeled MORB; however, this requires generally higher  $D$ 's to maintain the proper slope for M- to HREE. To get to  $F=10\%$ , at least another 30% fractionation is necessary and this seems unlikely. This low value for  $F$ , as compared to previous models, may be due to the fact that older estimates are based on anhydrous melting. Water content in the upper mantle is increasingly recognized as a very important aspect of mantle viscosity and convection [67] as well as mantle melting [68–71]. To test the validity of 6% mean  $F$ , we apply our estimated concentration of  $H_2O$  to the recent model by Asimow et al. [70] for hydrous mantle melting (the pHMELTS model).

A pHMELTS model run, using 110 ppm water, the major element compositions in Table 3, a potential temperature of 1360 °C, a 2-D passive triangle melting regime, and near-fractional melting, results in 7.0% mean melting to produce MORB and a crustal thickness of 6.3 km (P. Asimow, pers. comm., 2004). This confirms that the mean degree of melting (as defined by Plank et al. [72]) for hydrous models is generally on the low side of previous estimates from anhydrous models.

For average DMM, the derived  $D$  values (Table 2) translate into 2–3% melt depletion from primitive mantle using either non-modal or modal fractional melting models. Because average DMM is only 2–3% melt depleted, but average MORB is generated by 6% melting, one or all of the following is implied: (1) the degree of melting was lower in the past, (2) the mantle is a cannibal, recycling some crust and lithosphere back into itself, (3) depleted mantle has exchanged with the less depleted mantle, or (4) MORB generation is not the process that depletes the mantle.

#### 4. Crust–mantle mass balance

Classic works based on continental crust and the depleted mantle being sole complementaries calculate that from 30% to 70% of the mantle is depleted according to isotope and parent/daughter constraints ([1], refs. therein). In the following paragraphs, we provide three different scenarios for the balance of chemical reservoirs in the silicate earth, with each scenario progressively involving additional reservoirs. We believe that using the entire trace element suite to assess the extent to which the silicate earth does or

does not mass-balance is a robust way to calculate relative proportions of reservoirs. The mass of the continental crust is fixed to be 0.6% the mass of the silicate Earth. For each scenario, the best estimates of reservoir masses along with uncertainty in the estimates are derived from a Monte Carlo simulation with  $10^5$  trials in which element concentrations for each reservoir are considered as normal random variables with means given as PUM normalized concentrations and  $1\sigma$  equal to 10%; in each trial, the relative reservoir masses are determined by a linear least-squares fit to the input parameters. Uncertainties are quoted as  $2\sigma$ .

Scenario 1 is our own mass-balance involving only DMM and the continental crust, meaning in what proportion do DMM and the continental crust have to be added in order to sum back to primitive mantle? Our calculations indicate that  $33\pm 3\%$  the mass of the silicate Earth has to be DMM, with the remainder being primitive mantle, to best balance the bulk continental crust composition as estimated by Rudnick and Fountain [62]. For this particular ‘reconstituted’ mantle, all elements sum to within 15% of the primitive mantle except Rb and Pb which are in excess by 28% and 21%, respectively. This scenario is no doubt overly simplistic. For one, there is no real evidence for the existence of a primitive mantle reservoir (see review by Van Keken et al. [73]). However, there is evidence for a lower mantle that is less depleted than DMM, but depleted nonetheless; this reservoir is implied from many OIB isotopic arrays and termed FOZO by Hart et al. [74]. If a depleted lower mantle were accounted for here, the DMM reservoir would be significantly smaller than 33% in order to allow for the moderate depletion of the lower mantle.

Scenario 2 is the mass-balance of DMM, continental crust, and recycled oceanic crust. The idea of a recycled MORB component in the mantle is corroborated by the observation that the major element composition of DMM cannot be balanced by continental crust alone (see Table 3). At  $43\pm 6\%$  DMM and  $2.0\pm 0.6\%$  parental N-MORB of Su and Langmuir [28], this scenario provides a better fit for most elements than does the first scenario; all elements here are fit to within 8% except Rb and Pb with 20% and 15% excesses and Nb with a 17% deficit. The abundance of MORB cannot be increased

greatly without having elevated M- to HREE that cannot be compensated by adding more DMM. However, we have not considered subduction zone alteration of oceanic crust, which almost certainly affects this mass balance.

Scenario 3 is the mass-balance of DMM, continental crust, recycled oceanic crust, and an OIB source component (from Workman et al. [75]). To show upper limits on the sizes of enriched mantle components, the mass balance calculation has been made assuming 0% primitive mantle. The resulting balance is  $74 \pm 5\%$  DMM,  $4.7 \pm 1.0\%$  MORB, and  $21 \pm 5\%$  OIB source; all elements are fit to within 15% except Rb and Nb with 23% excess and 21% deficit, respectively.

In each scenario 2 and 3, the fraction of MORB in the mass-balance is less than the mass of oceanic crust generated throughout Earth history (6–7% of the mantle mass, assuming constant rates for 4.55 Ga). As such, it is suggestive of the mantle being partially cannibalistic with respect to subducted oceanic crust. However, these mass balances do not include a depleted lithosphere, and could therefore be misrepresentative if oceanic crust and lithosphere are shown to be absolutely mechanically and thermally coupled.

## 5. Conclusions

Through abyssal peridotite trends, the isotopic composition of N-MORB and a few canonical ratios, we have constructed a major and trace element reference model for average, unmelted, depleted MORB mantle (DMM). From this DMM, parental MORB is generated by about 6% aggregated fractional melting as constrained primarily from the enrichment factor for the highly incompatible elements in parental MORB. Melting occurs mainly in the spinel facies mantle, but is most likely initiated within the uppermost garnet facies, as suggested by pHMELTS model runs. The water content inferred by the derived trace element composition is between 70 and 160 ppm, and is an integral ingredient in modeling mantle melting [70] and mantle viscosity [67,68]. We have provided trace element compositions for minerals in the uppermost mantle which can be better estimated in the future with increasingly accurate information on mineral/mineral partitioning of trace elements and

compositional variations of minerals with temperature and pressure.

The radiogenic heat production of DMM (from U, Th, and K) is only 15% that of the bulk silicate Earth at  $2.43 \times 10^{-9}$  W/m<sup>3</sup>, using a density of 3.20 g/cm<sup>3</sup> and radiogenic heat production values from Durrance [76]. It takes ~33% of the mantle mass to be composed of DMM, the remaining being primitive mantle, to balance the continental crust alone, and ~43% if including an oceanic crust component. If there is no primitive mantle, the maximum masses of the oceanic crust and OIB reservoirs are 5% and 21%, respectively, if these enriched reservoirs are balanced purely by DMM.

Overall, the composition constructed here is a robust estimate for average upper mantle and can be used as an input parameter for a variety of models concerning mantle processes.

## Acknowledgements

We are endlessly grateful to Henry Dick, whose decades of toils over mid-ocean ridges and abyssal peridotites have made possible the work presented here; in jest we question his sanity for counting over half a million points on abyssal peridotite modal abundances. Many stimulating conversations have been had with Nobu Shimizu, Jessica Warren, Glenn Gaetani, Peter Kelemen, and Greg Hirth on the nature of the depleted mantle. We especially thank Paul Asimow for a sneak-preview application of his new pHMELTS model, as well as E. Hauri and W. McDonough for their helpful reviews.

## Appendix A. Supplementary data

Supplementary data associated with this article can be found, in the online version, at [doi:10.1016/j.epsl.2004.12.005](https://doi.org/10.1016/j.epsl.2004.12.005).

## References

- [1] C.J. Allègre, S.R. Hart, J.F. Minster, Chemical structure and evolution of the mantle and the continents determined by inversion of Nd and Sr isotopic data: II. Numerical experiments and discussion, *Earth Planet. Sci. Lett.* 66 (1983) 191–213.

- [2] J.J.G. Galer, R.K. O’Nions, Residence time of thorium, uranium and lead in the mantle and implications for mantle convection, *Nature* 316 (1985) 778–782.
- [3] F. Albarede, M. Brouxel, The Sm/Nd secular evolution of the continental crust and depleted mantle, *Earth Planet. Sci. Lett.* 82 (1987) 25–35.
- [4] N. Shimizu, The geochemistry of olivine-hosted melt inclusions in a FAMOUS basalt ALV519-4-1, *Phys. Earth Planet. Inter.* 107 (1998) 183–201.
- [5] T. Elliott, A. Zindler, B. Bourdon, Exploring the kappa conundrum: the role of recycling in the lead isotope evolution of the mantle, *Earth Planet. Sci. Lett.* 169 (1999) 129–145.
- [6] V.J.M. Salters, A. Stracke, The composition of the depleted mantle, *Geochem. Geophys. Geosyst.* 5 (5) (2004) doi:10.1029/2003GC000597.
- [7] D. McKenzie, R.K. O’Nions, Partial melt distributions from inversion of rare earth element concentrations, *J. Pet.* 32 (1991) 1021–1091.
- [8] A.W. Hofmann, Chemical differentiation of the Earth: the relationship between mantle, continental crust, and oceanic crust, *Earth Planet. Sci. Lett.* 90 (1988) 297–314.
- [9] S.-s. Sun, W.F. McDonough, Chemical and isotopic systematics of oceanic basalts: implications for mantle composition and processes, in: A.D. Saunders, M.J. Norry (Eds.), *Magma-tism in the Ocean Basins*, Geological Society, London, 1989, pp. 313–345.
- [10] K.T.M. Johnson, H.J.B. Dick, N. Shimizu, Melting in the oceanic upper mantle; an ion microprobe study of diop-sides in abyssal peridotites, *J. Geophys. Res.* 95 (1990) 2661–2678.
- [11] K.T.M. Johnson, H.J.B. Dick, Open system melting and temporal and spatial variation of peridotite and basalt at the Atlantis II fracture zone, *J. Geophys. Res.* 97 (1992) 9219–9241.
- [12] M. Loubet, N. Shimizu, C.J. Allegre, Rare Earth elements in alpine peridotites, *Contrib. Mineral. Petrol.* 53 (1975) 1–12.
- [13] S.R. Hart, A. Zindler, In search of a bulk-earth composition, *Chem. Geol.* 57 (1986) 247–267.
- [14] W.F. McDonough, S.-s. Sun, The composition of the Earth, *Chem. Geol.* 120 (1995) 223–253.
- [15] H.J.B. Dick, R.L. Fisher, W.B. Bryan, Mineralogical variability of the uppermost mantle along mid-ocean ridges, *Earth Planet. Sci. Lett.* 69 (1984) 88–106.
- [16] H.J.B. Dick, Abyssal-peridotites, very slow spreading ridges and oceanic ridge magmatism, in: A.D. Saunders, M.J. Norry (Eds.), *Magma-tism in the Ocean Basins*, Geological Society, London, 1989, pp. 71–105.
- [17] P.B. Kelemen, H.J.B. Dick, J.E. Quick, Formation of harzburgite by pervasive melt/rock reaction in the upper mantle, *Nature* 358 (1992) 635–641.
- [18] H.J.B. Dick, J.H. Natland, Late-stage melt evolution and transport in the shallow mantle beneath the East Pacific Rise, in: C. Mevel, K.M. Gillis, J.F. Allan, P.S. Meyer (Eds.), *Proceedings of the Ocean Drilling Program. Scientific Results*, vol. 147, 1996, pp. 103–134.
- [19] E. Hellebrand, J.E. Snow, P. Hoppe, A.W. Hofmann, Garnet-field melting and late-stage refertilization in ‘residual’ abyssal peridotites from the Central Indian Ridge, *J. Petrol.* 43 (2002) 2305–2338.
- [20] V.J.M. Salters, H.J.B. Dick, Mineralogy of the mid-ocean ridge basalt source from neodymium isotopic composition in abyssal peridotites, *Nature* 418 (2002) 68–72.
- [21] P. Tartarotti, S. Susini, P. Nimis, L. Ottolini, Melt migration in the upper mantle along the Romanche Fracture Zone (Equatorial Atlantic), *Lithos* 63 (2002) 125–149.
- [22] P.B. Kelemen, G.M. Yogodzinski, D.W. Scholl, Along-strike variation in lavas of the Aleutian island arc: implications for the genesis of high Mg# andesite and the continental crust, in: J. Eiler (Ed.), *Inside the Subduction Factory*, AGU Monograph, vol. 138, AGU, Washington, DC, 2004, pp. 223–276.
- [23] H. Zou, Trace element fractionation during modal and nonmodal dynamic melting and open-system melting: a mathematical treatment, *Geochim. Cosmochim. Acta* 62 (1998) 1937–1945.
- [24] D. York, Least-squares fitting of a straight line, *Can. J. Phys.* 44 (1966) 1079–1086.
- [25] A. Zindler, S.R. Hart, Chemical geodynamics, *Annu. Rev. Earth Planet. Sci.* 14 (1986) 493–571.
- [26] S.R. Hart, Heterogeneous mantle domains: signatures, genesis and mixing chronologies, *Earth Planet. Sci. Lett.* 90 (1988) 273–296.
- [27] A.W. Hofmann, Mantle geochemistry: the message from oceanic volcanism, *Nature* 385 (1997) 219–229.
- [28] Y. Su, C.H. Langmuir, Global MORB chemistry compilation at the segment scale, PhD Thesis, Department of Earth and Environmental Sciences, Columbia University, 2003. Available at: <http://petdb.ldeo.columbia.edu/documentation/morbcompilation/>.
- [29] G.M. Nowell, P.D. Kempton, S.R. Noble, J.G. Fitton, A.D. Saunders, J.J. Mahoney, R.N. Taylor, High precision Hf isotope measurements of MORB and OIB by thermal ionization mass spectrometry: insights into the depleted mantle, *Chem. Geol.* 149 (1998) 211–233.
- [30] C. Chauvel, J. Blichert-Toft, A hafnium isotope and trace element perspective on melting of the depleted mantle, *Earth Planet. Sci. Lett.* 190 (2001) 137–151.
- [31] M. Andres, J. Blichert-Toft, J. Schilling, Hafnium isotopes in basalts from the southern Mid-Atlantic Ridge from 40°S to 55°S: discovery and Shona plume-ridge interactions and the role of recycled sediments, *Geochem. Geophys. Geosyst.* 3 (2002).
- [32] P.M. Hurley, J.R. Rand, Pre-drift continental nuclei, *Science* 164 (1969) 1229–1242.
- [33] R.L. Armstrong, A model for the evolution of strontium and lead isotopes in a dynamic earth, *Rev. Geophys.* 6 (1968) 175–199.
- [34] R.L. Armstrong, Radiogenic isotopes: the case for crustal recycling on a near-steady-state no-continental-growth Earth, *Philos. Trans. R. Soc. Lond.* 301 (1981) 443–472.
- [35] W.S. Fyfe, The evolution of the Earth’s crust; modern plate tectonics to ancient hot spot tectonics, *Chem. Geol.* 23 (1978) 89–114.
- [36] M.T. McCulloch, V.C. Bennett, Progressive growth of the Earth’s continental crust and depleted mantle; geochem-

- ical constraints, *Geochim. Cosmochim. Acta* 58 (1994) 4717–4738.
- [37] S.R. Taylor, S.M. McLennan, The geochemical evolution of the continental crust, *Rev. Geophys.* 33 (1995) 241–265.
- [38] K.C. Condie, Episodic continental growth models: afterthoughts and extensions, *Tectonophysics* 322 (2000) 153–162.
- [39] S.A. Bowring, T. Housh, The Earth's early evolution, *Science* 269 (1995) 1535–1540.
- [40] J.D. Vervoort, P.J. Patchett, G.E. Gehrels, A.P. Nutman, Constraints on early Earth differentiation from hafnium and neodymium isotopes, *Nature* 379 (1996) 624–627.
- [41] C.J. Allègre, Comportement des systèmes U–Th–Pb dans le manteau supérieur et modèle d'évolution de ce dernier au cours des temps géologiques, *Earth Planet. Sci. Lett.* 5 (1969) 261–269.
- [42] S.R. Hart, C. Brooks, Rb–Sr mantle evolution models, *Year b. Carnegie Inst.* 68 (1970) 426–429.
- [43] M. Tatsumoto, Genetic relations of oceanic basalts as indicated by lead isotopes, *Science* 153 (1996) 1094–1101.
- [44] C.C. Lundstrom, D.E. Sampson, M.R. Perfit, J. Gill, Q. Williams, Insights into mid-ocean ridge basalt petrogenesis: U-series disequilibria from the Siqueiros Transform, Lamont Seamounts, and the Pacific Rise, *J. Geophys. Res.* 104 (1999) 13035–13048.
- [45] K.W.W. Sims, S.J. Goldstein, J. Blichert-Toft, M.R. Perfit, P. Kelemen, D.J. Fornari, P. Michael, M.T. Murrell, S.R. Hart, D.J. DePaolo, G.D. Layne, L.A. Ball, M. Jull, J. Bender, Chemical and isotopic constraints on the generation and transport of magma beneath the East Pacific rise, *Geochim. Cosmochim. Acta* 66 (2002) 3481–3504.
- [46] K.W.W. Sims, J. Blichert-Toft, D.J. Fornari, M.R. Perfit, S.J. Goldstein, P. Johnson, D.J. DePaolo, S.R. Hart, M.T. Murrell, P.J. Michael, G.D. Layne, L.A. Ball, Aberrant youth: chemical and isotopic constraints on the origin of off-axis lavas from the East Pacific Rise, 9°–10°N, *Geochem. Geophys. Geosyst.* 4 (2003).
- [47] A.W. Hofmann, W.M. White, Ba, Rb and Cs in the Earth's mantle, *Z. Naturforsch.* 38 (1983) 256–266.
- [48] A.W. Hofmann, K.P. Jochum, H.M. Seufert, W.M. White, Nb and Pb in oceanic basalts: new constraints on mantle evolution, *Earth Planet. Sci. Lett.* 79 (1986) 33–45.
- [49] K.P. Jochum, J.A. Pfänder, J.E. Snow, A.W. Hofmann, Nb/Ta in mantle and crust, *EOS* 78 (1997) F805.
- [50] K.W.W. Sims, D.J. DePaolo, Inferences about mantle magma sources from incompatible trace element concentration ratios in oceanic basalts, *Geochim. Cosmochim. Acta* 61 (1997) 765–784.
- [51] J.A. Pfänder, C. Münker, K. Mezger, A.W. Hofmann, In search of a superchondritic Nb/Ta reservoir: high-precision Nb/Ta and Zr/Hf ratios in ocean island and interplate basalts, *Abstr.-Goldschmidt Conf.* 66 (2002) A597.
- [52] S. Weyer, C. Münker, M. Rehkamper, K. Mezger, Determination of ultra-low Nb, Ta, Zr and Hf concentrations and the chondritic Zr/Hf and Nb/Ta ratios by isotope dilution analyses with multiple collector ICP-MS, *Chem. Geol.* 187 (2002) 295–313.
- [53] P. Michael, Regionally distinctive sources of depleted MORB: evidence from trace elements and H<sub>2</sub>O, *Earth Planet. Sci. Lett.* 131 (1995) 301–320.
- [54] A. Saal, Vapor undersaturation in primitive mid-ocean-ridge basalt and the volatile content of Earth's upper mantle, *Nature* 419 (2002) 451–455.
- [55] P.J. Michael, E. Bonatti, Peridotite compositions from the North Atlantic: regional and tectonic variations and implications for partial melting, *Earth Planet. Sci. Lett.* 73 (1985) 91–104.
- [56] Y. Niu, C.H. Langmuir, R.J. Kinzler, The origin of abyssal peridotites: a new perspective, *Earth Planet. Sci. Lett.* 152 (1997) 251–265.
- [57] M.B. Baker, J.R. Beckett, The origin of abyssal peridotites: a reinterpretation of constraints based on primary bulk compositions, *Earth Planet. Sci. Lett.* 171 (1999) 49–61.
- [58] R.J. Kinzler, T.L. Grove, Primary magmas of mid-ocean ridge basalts: 1. Experiments and methods, *J. Geophys. Res.* 97 (1992) 6885–6906.
- [59] M.J. Walter, T.W. Sisson, D.C. Presnall, A mass proportion method for calculating melting reactions and application to melting of model upper mantle lherzolite, *Earth Planet. Sci. Lett.* 135 (1995) 77–90.
- [60] G.A. Gaetani, T.L. Grove, The influence of water on melting of mantle peridotite, *Contrib. Mineral. Petrol.* 131 (1998) 323–346.
- [61] M.M. Hirschmann, M.S. Ghiorso, L.E. Waslylenki, P.D. Asimow, E.M. Stolper, Calculation of peridotite partial melting from thermodynamic models of minerals and melts: I. Review of methods and comparison with experiments, *J. Petrol.* 39 (1998) 1091–1115.
- [62] R.L. Rudnick, D.M. Fountain, Nature and composition of the continental crust: a lower crustal perspective, *Rev. Geophys.* 33 (1995) 267–309.
- [63] E. Hauri, S.R. Hart, Rhenium abundances and systematics in oceanic basalts, *Chem. Geol.* 139 (1997) 185–205.
- [64] A.V. Sobolev, N. Shimizu, Ultra-depleted primary melt included in an olivine from the Mid-Atlantic Ridge, *Nature* 363 (1993) 151–154.
- [65] C.H. Langmuir, E.M. Klein, T. Plank, Petrological systematics of mid-ocean ridge basalts: constraints on melt generation beneath ocean ridges, in: J.P. Morgan, D.K. Blackman, J.M. Sinton (Eds.), *Mantle Flow and Melt Generation at Mid-ocean Ridges*, *Geophys. Monogr. Ser.*, vol. 71, AGU, Washington, DC, 1992, pp. 180–183.
- [66] R.J. Kinzler, T.L. Grove, Primary magmas of mid-ocean ridge basalts: 2. Applications, *J. Geophys. Res.* 97 (1992) 6907–6926.
- [67] G. Hirth, D.L. Kohlstedt, Rheology of the upper mantle and the mantle wedge: a view from the experimentalists, in: J. Eiler (Ed.), *Inside the Subduction Factory*, *AGU Monograph*, vol. 138, AGU, Washington, DC, 2004, pp. 83–105.
- [68] G. Hirth, D.L. Kohlstedt, Water in the oceanic upper mantle: implications for rheology, melt extraction, and the evolution of the lithosphere, *Earth Planet. Sci.* 144 (1996) 93–108.
- [69] P.D. Asimow, C.H. Langmuir, The importance of water to oceanic mantle melting regimes, *Nature* 421 (2003) 815–820.

- [70] P.D. Asimow, J.E. Dixon, C.H. Langmuir, A hydrous melting and fractionation model for mid-ocean ridge basalts: application to the Mid-Atlantic Ridge near the Azores, *Geochem. Geophys. Geosyst.* 5 (2004).
- [71] S.W. Parman, T.L. Grove, Harzburgite melting with and without H<sub>2</sub>O: experimental data and predictive modeling, *J. Geophys. Res.* 109 (2004).
- [72] T. Plank, M. Spiegelman, C.H. Langmuir, D.W. Forsyth, The meaning of “mean F”: clarifying the mean extent of melting at ocean ridges, *J. Geophys. Res.* 100 (1995) 15045–15052.
- [73] P.E. Van Keken, E.H. Hauri, C.J. Ballentine, Mantle mixing: the generation, preservation, and destruction of chemical heterogeneity, *Annu. Rev. Earth Planet. Sci.* 30 (2002) 493–525.
- [74] S.R. Hart, E.H. Hauri, L.A. Oschmann, J.A. Whitehead, Mantle plumes and entrainment: isotopic evidence, *Science* 256 (1992) 517–520.
- [75] R.K. Workman, S.R. Hart, M. Jackson, M. Regelous, K.A. Farley, J. Blusztajn, M. Kurz, H. Staudigel, Recycled metasomatized lithosphere as the origin of the enriched mantle II (EM2) endmember: evidence from the Samoan Volcanic chain, *Geochem. Geophys. Geosyst.* 5 (2004).
- [76] E.M. Durrance, *Radioactivity on Geology: Principles and Applications*, Ellis Horwood, Chichester, 1986.
- [77] A.P. Dickin, *Radiogenic Isotope Geology*, Cambridge University Press, Cambridge, UK, 1995. 490 pp.
- [78] D.C. Presnall, J.D. Hoover, High pressure phase equilibrium constraints on the origin of mid-ocean ridge basalts, in: B.O. Mysen (Ed.), *Magmatic Processes: Physicochemical Principles*, Special Publication-Geochemical Society, vol. 1, 1987, pp. 75–89.